LAWRENCE
LIVERMORE
NATIONAL
LABORATORY

LLNL-JRNL-498898

Nonlinear effects in the combined Rayleigh-Taylor/Kelvin-Helmholtz instability

B. J. Olson, S. K. Lele, J. Larsson, A. W. Cook

September 12, 2011

Physics of Fluids

Disclaimer

Nonlinear effects in the combined Rayleigh-Taylor/Kelvin-Helmholtz instability

Britton J. Olson* and Sanjiva K. Lele
Department of Aeronautics and Astronautics, Stanford University, Stanford, CA 94305, USA

Johan Larsson
Center for Turbulence Research, Stanford University, Stanford, CA 94305, USA

Andrew W. Cook
Lawrence Livermore National Laboratory, Livermore, CA 94551-0808, USA

The combined Rayleigh-Taylor/Kelvin-Helmholtz instability is studied in the early nonlinear regime. Specifically, the effect of adding mean shear to a gravitationally unstable configuration is investigated. While linear stability theory predicts that any amount of mean shear would increase the growth rate beyond the Rayleigh-Taylor value, numerical (large eddy) simulations show a more complex and non-monotonic behavior where small amounts of mean shear in fact decrease the growth rate. A velocity scale for the combined instability is proposed from linear stability arguments, and is shown to effectively collapse the growth rates for different configurations. The specific amount of mean shear that minimizes the peak growth rate is identified, and the physical origins of this non-monotonic behavior are investigated.

I. INTRODUCTION

The canonical Rayleigh-Taylor (RT) instability is driven by a misalignment of the density gradient and the pressure gradient induced by a body force (e.g., gravity or system acceleration). With heavier fluid initially sitting atop lighter fluid under downward gravitational force, perturbations on the unstable interface begin to grow. The canonical Kelvin-Helmholtz (KH) instability, on the other hand, occurs at the shear layer between two fluids with different horizontal velocities. These instabilities, both individually and combined, are of great interest in plasma physics applications such as Inertial Confinement Fusion (ICF) and Type-1a supernovae collapse. For example, the spherical interface of a fusion capsule can become RT unstable and fail to contain the fusion reaction adequately [5].

The combined RT/KH problem considered in this study is sketched in Fig. 1. An initially thin interface in the $x-y$ plane separates the upper and lower fluids with densities ρ_1 and ρ_2, respectively, where $\rho_1 > \rho_2$. The Atwood number is defined as $A \equiv (\rho_1 - \rho_2) / (\rho_1 + \rho_2)$. The interface is perturbed with characteristic wavelength λ_0. The gravitational acceleration g acts in the negative z direction, while the imposed velocity difference ΔV acts in the x direction. Fig. 2 shows differences in the mixing layer evolution as shear is incrementally added to the RT unstable

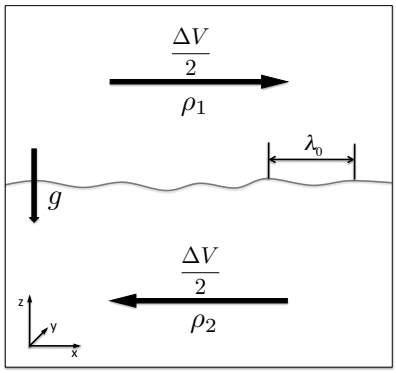

FIG. 1: Sketch of the combined Rayleigh-Taylor/Kelvin-Helmholtz (RT/KH) instability.

*Britton J. Olson: bolson@stanford.edu

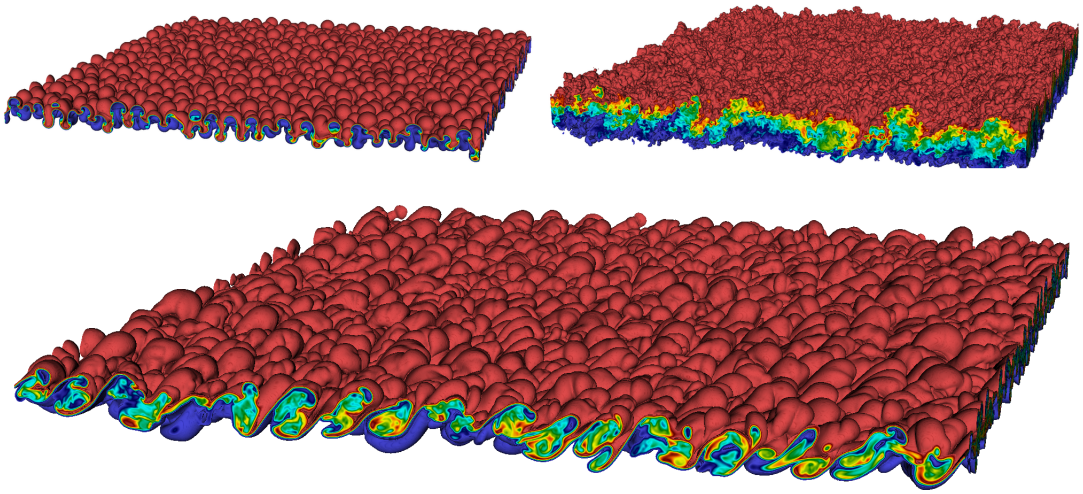

FIG. 2: Isovolumes of density showing differences between the unstable interface in a pure RT (upper left), a high shear (upper right) and an intermediate shear case.

configuration. This setup is identical, omitting the magnetic field, to the case studied by Zang et al[12]. It also models the experiment performed by Snider and Andrews [13], where hot and cold streams of water at different speeds mix past the edge of a splitter plate.

Several studies in the literature (e.g., [1–3, 11, 12]) address the combined RT/KH problem through linear stability analysis. For a sharp interface, the linear analysis involves solutions of the form

$$\psi(x,y,z,t) = \hat{\psi}(z)\exp\left[\gamma t + i(k_x x + k_y y - \omega t)\right] , \quad \psi = \rho, u, v, w ,$$
$$\eta(x,y,t) = \hat{\eta}\exp\left[\gamma t + i(k_x x + k_y y - \omega t)\right] ,$$

where $\eta(x,y,t)$ is the height of the perturbed interface. The growth rate is

$$\gamma = \sqrt{\frac{1-A^2}{4}\Delta V_x^2 k^2 + Agk} , \quad \Delta V_x = \frac{k_x}{k}\Delta V , \tag{1}$$

where $k = \sqrt{k_x^2 + k_y^2}$ is the magnitude of the wave vector and the reduced velocity-difference ΔV_x has been introduced for modes not aligned with the imposed shear. The prediction of linear stability theory is clearly that, for given parameters (A, g, k) specifying the RT-problem, the linear growth rate γ increases monotonically with the imposed shear ΔV. As will be shown below, this is not true in the nonlinear regime.

The fact that applied shear can decrease the RT growth rate has been observed in prior studies by Guzdar et. al. [3] and later by Shumlak and Roderick[11]. These studies used analytical density and velocity profiles with finite interface widths which are on the order of the initial disturbance wavelength. In both cases, linear stability theory predicts the stabilization of the RT interface by the addition of shear flow. In our case, however, we use a discontinuous interface between two uniform states of density and horizontal velocity. This configuration represents a special case in the prior analysis where the interface thickness goes to zero. In such a case, as we have seen, LST does not predict a stabilization of the RT interface.

In the present study we focus on the early nonlinear regime before full transition to turbulence. Large eddy simulation (LES) is used to compute the evolution into the nonlinear regime. The accuracy of the LES is established by comparison to direct numerical simulation (DNS) and a suite of verification problems, where the effects of finite resolution, box size, and statistical sampling size, are presented.

II. METHODOLOGY

The governing equations for two incompressible miscible fluids with a gravitational body force are (cf. Ref. [8])

$$\frac{\partial \rho}{\partial t} + u_j \frac{\partial \rho}{\partial x_j} = -\rho \frac{\partial u_j}{\partial x_j} = \rho \frac{\partial}{\partial x_j}\left(\frac{D}{\rho}\frac{\partial \rho}{\partial x_j}\right), \tag{2a}$$

$$\frac{\partial \rho u_i}{\partial t} + \frac{\partial \rho u_i u_j}{\partial x_j} = \rho g_i - \frac{\partial p}{\partial x_i} + \frac{\partial \tau_{ij}}{\partial x_j}, \tag{2b}$$

where

$$\tau_{ij} = \mu\left[\frac{\partial u_i}{\partial x_j} + \frac{\partial u_j}{\partial x_i} - \frac{2}{3}\delta_{ij}\frac{\partial u_k}{\partial x_k}\right]$$

is the viscous stress tensor and μ is the shear viscosity. The species diffusivity D gives rise to a non-solenoidal flow [6].

Gravity acts in the negative z direction while the imposed velocity difference is in the x direction. The horizontal x and y directions are periodic. The initial interface height $\eta(x, y, 0)$ is taken as random with the Gaussian spectrum

$$E_\eta(k) \sim \exp\left[-(k-k_0)^2/(2\sigma^2)\right], \tag{3}$$

where k_0 is the wavenumber at peak energy; this is taken as corresponding to the 24th mode in the periodic x and y directions. The width of the Gaussian is set by taking $\sigma^2 = k_0^2/9$. The length scale of the peak initial perturbation is defined as $\lambda_0 \equiv 2\pi/k_0$.

The mixing rate is computed as the time-derivative $\dot{h}(t)$ of the interface thickness $h(t)$, which is defined here following Cabot and Cook [8] as

$$h(t) \equiv \int_{-\infty}^{\infty} 2\min\left\{\frac{\overline{\rho}(z,t) - \rho_L}{\Delta\rho}, \frac{\rho_H - \overline{\rho}(z,t)}{\Delta\rho}\right\} dz, \tag{4}$$

where $\overline{\rho}(z,t)$ implies an average over the horizontal directions and $\Delta\rho \equiv \rho_H - \rho_L$ is the density difference.

The equations are solved using a 10th-order compact central difference scheme for spatial derivatives, and integrated in time using a 3rd-order Adams-Bashforth-Moulton predictor corrector method[7]. The Reynolds number is defined as $Re \equiv h\dot{h}/\nu$, and the Schmidt number was set to $Sc = 0.7$.

The present study is focused on instability and mixing in the high-Reynolds number regime where the viscous length scales are significantly smaller than the energy-containing structures. We thus consider relatively high Reynolds numbers of $Re = h\dot{h}/\nu \approx 15000$ in this study, and close the equations with subgrid terms following Cook [9]. The numerical method and the LES regularization model were chosen to maximize the range of scales captured and to minimize the numerical dissipation.

For this problem of miscible fluids, and to minimize numerical errors at the early times, the initial interface is specified as diffuse using a hyperbolic tangent function. The thickness of the diffuse interface is one order of magnitude smaller than the dominant wavelength λ_0. To test whether the finite thickness has an effect on the result, a simulation where the interface was thickened by 20% was run; this caused less than 2% difference in the resulting mixing-height growth rate $\dot{h}$.

A. Effect of finite grid resolution

To verify the resulting LES methodology, we consider a case at lower Re which is accessible to DNS. The key results from this comparison with DNS are shown in Fig. 3 for a sequence of LES grids. Grid resolution is defined by the number of grid points per initial perturbation wave length $N = \Delta/\lambda_0$. This value is set to (11, 21, 43, 64) for the coarse, medium, fine and very fine grids, respectively. We note that the Reynolds number of the finest case is about 4000 by the end of the calculation, which places it in the transitional regime, according to the finding of Cabot and Cook [8]. All cases for the convergence study were run in the "high-shear" configuration, where the shear velocity scale was much larger than the RT-velocity scale, viz., $\Delta V/\sqrt{Ag\lambda_0} \approx 6$, where $A = 0.5$. This is a shear-dominated case and was found to have the most stringent resolution requirements amongst the range of parameters studied.

The mixing rate $\dot{h}$ from the LES converges to the DNS for grids with at least 21 points per characteristic wavelength λ_0. The vertical profile of kinetic energy at the time of peak growth rate converges to the DNS for grids with at least 43 points per λ_0. We thus use 43 points per wavelength in the present study, which is more resolved than the DNS in Ref. [8] (32 points per wavelength). The agreement between LES and DNS is expected, since the flow at these relatively early times has not yet become fully turbulent. Moreover, the entrainment rate is determined by large structures, which are captured directly in the LES provided that the grid is sufficiently fine.

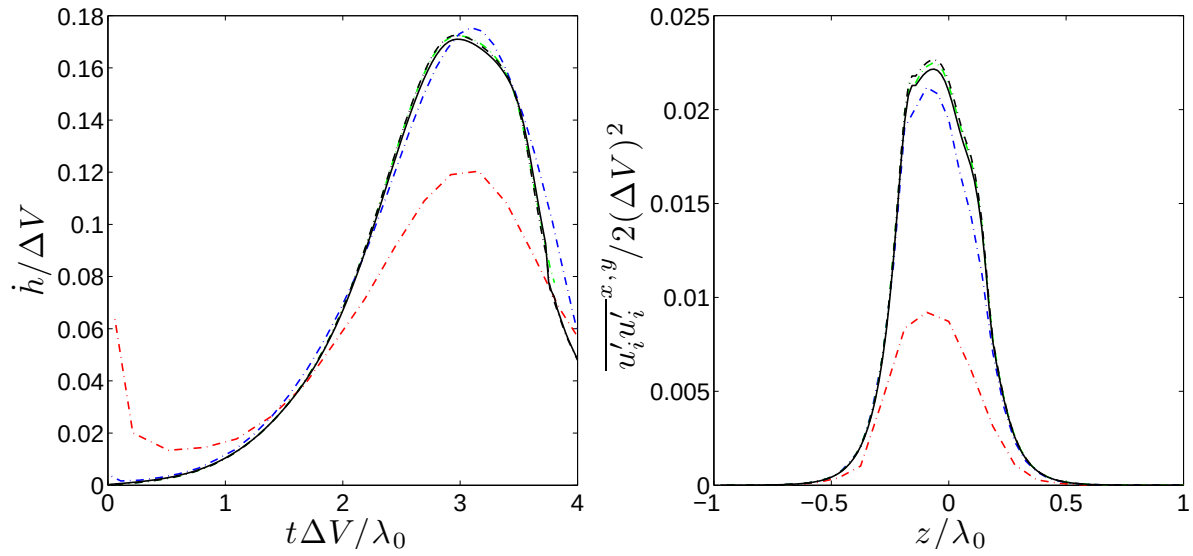

FIG. 3: Comparison of DNS and LES on a sequence of grids. Left: Growth rate of the mixing interface $\dot{h}$ and plane-averaged turbulent kinetic energy at the time of peak growth rate $t\Delta V/\lambda_0 = 3$. Right: DNS with 64 points per initial perturbation wave length (solid black line); LES with 64 (dashed black), 43 (green dashed), 21 (blue dashed), and 11 (red dashed) points per initial perturbation wave length.

k_0	Sampling error (ϵ_{ss})	Box size error (ϵ_{bs})
6	.0613	.0347
12	.0419	.0172
24	.0260	-

TABLE I: Table of errors in maximum mixing growth rate ($\dot{h}_{\mathbf{max}}$) for varying box sizes ($E_{bs}(k_0)$) and sample size ($E_{ss}(k_0)$).

B. Effect of finite box size

The box size of the simulations must be sufficiently large such that the effects of the periodic boundaries do not affect the statistics. That is, in wave space, there must be sufficient room in the direction of decreasing wave numbers for energy to move. We verify that a sufficiently large domain is used by comparing solutions obtained from three box sizes. For each box size, three independent (but statistically equivalent) initial fields were used to start the calculation and their averages were compared against the reference solution (the largest domain). Although this is an approximation, we obtain a clear picture of the convergent behavior as the box size increases. Table I lists the relative error in the peak growth rate, defined as

$$\epsilon_{bs}\left(k_0\right) \equiv \frac{\left|\overline{\dot{h}_{max}}|_{ref} - \overline{\dot{h}_{max}}|_{k_0}\right|}{\overline{\dot{h}_{max}}|_{ref}} \,, \tag{5}$$

where $\dot{h}_{max} = max\left\{\dot{h}(t)\right\}$, $\overline{\dot{h}_{max}}$ is the mean of the three cases at given k_0, $|\cdot|$ is the absolute value and "ref" is the reference solution. As seen in the table, the error due to the finite box size is at most a few percent.

C. Effect of finite statistical sampling

The final criteria used to validate the fidelity of our simulations is that of statistical convergence. Any two initial fields will vary by a random phases but will have identical spectra as given by Eqn. 3. Therefore, sufficiently many samples of the characteristic large structure size λ_0 are needed to give results that are independent of the randomness in the initial condition. Sampling size error is defined as:

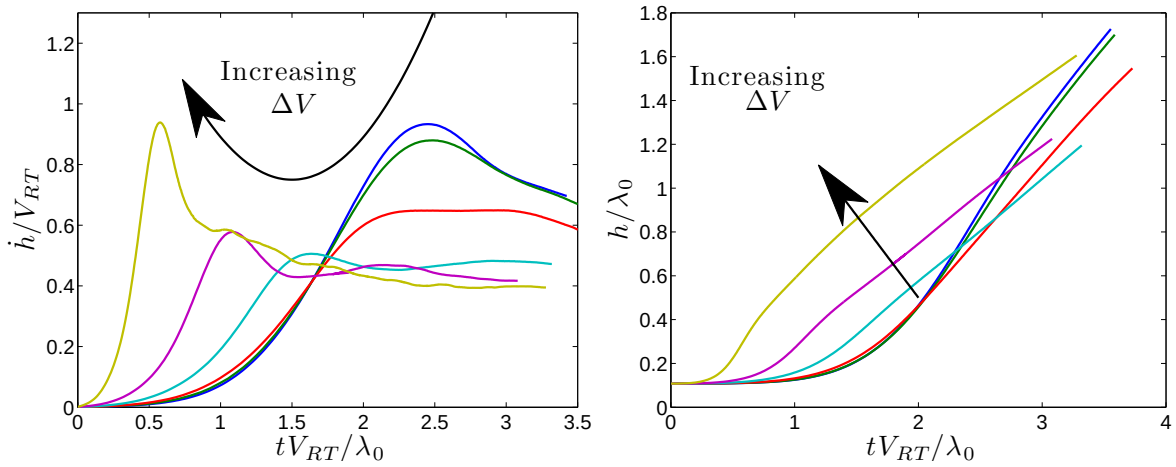

FIG. 4: Combined RT/KH instability with fixed RT-parameters (A, g, λ_0) but varying amounts of shear ΔV, with $A = 0.5$. Mixing rate $\dot{h}$ (left) and interface thickness h (right) of the layer as functions of time. Note that the axes are scaled using the characteristic velocity scale for the RT-problem, $V_{RT} = \sqrt{Ag\lambda_0}$. In order of increasing shear, the lines have $\Delta V/V_{RT}$ of 0 (blue), 0.3 (green), 0.9 (red), 1.8 (cyan), 3.1 (magenta), and 6.1 (yellow).

$$\epsilon_{ss}\left(k_0\right) \equiv \left. \frac{\sum_{i=1}^{N} \left(\left| \overline{\dot{h}_{max}} - \left(\dot{h}_{max}\right)_i \right| \right)}{N \overline{\dot{h}_{max}}} \right|_{k_0} \tag{6}$$

where $N = 3$ is the number of independent realizations and $\dot{h}_{max}|_i$ is the value for each realization. The sampling error decreases for increasing k_0, and is found to be 2.6% for $k_0 = 24$.

From Table I, we conclude that k_0, corresponding to mode 24, is sufficient to minimize the effect of the finite box size and sampling error to an acceptable level. Together with the requirement of having 43 points per characteristic wavelength, the final grids use 1024×1024 points in the horizontal directions. With isotropic grid spacing, we take 256 points in the z direction.

III. MIXING RATES FOR COMBINED RT/KH IN NONLINEAR REGIME

Consider a problem with fixed RT-parameters (A, g, λ_0) but with varying amounts of shear, i.e., with varying ΔV. Figure 4 shows the computed mixing rates $\dot{h}$ versus time for such a problem. The amount of shear is varied in the figure from none (pure RT) to a very large value(essentially pure KH). Adding an excessive amount of shear clearly accelerates the mixing as the flow then develops as a KH instability which is characterized by a different time scale. The linear stability analysis suggests that adding any amount of shear will increase the growth rate, γ, of the instability. For the spectra given in equation 3, $\gamma(k_0)$ has a linear relationship to the mixing rate, $\dot{h}$. Therefore, linear stability predicts a monotonic increase for the mixing rate with shear addition. However, figure 4 clearly shows that this is not the case: the case with moderate shear instead has a lower growth rate than the pure RT case. This surprising result raises several questions. First, what is the physical mechanism by which the addition of shear velocity diverts or delays the RT instability? Secondly, at what point is this unexpected effect of shear velocity most pronounced for a given set of parameters defining RT? That is, what is the optimal amount of shear needed to minimize this early time mixing rate?

As a prelude to investigating these questions, we first note that the mixing rate $\dot{h}$ and time t in Fig. 4 are scaled by velocity and time scales characteristic of pure RT problems, i.e., a velocity scale $V_{RT} = \sqrt{Ag\lambda_0}$ and time scale $T_{RT} = \lambda_0/V_{RT}$. While a pure KH problem would have the same characteristic length scale, λ_0, it would have the velocity scale $V_{KH} = \Delta V$. It is, at this stage, not clear what velocity scale to use for the combined problem, other than that the combined velocity scale V_{RTKH} should tend to V_{RT} as $\Delta V \to 0$ and V_{KH} as $\Delta V \to \infty$.

While linear stability theory misses the non-monotonic change in growth rate with the addition of shear, we can still use linear stability to guide the choice of the combined velocity scale V_{RTKH}. Dividing the linear growth rate γ

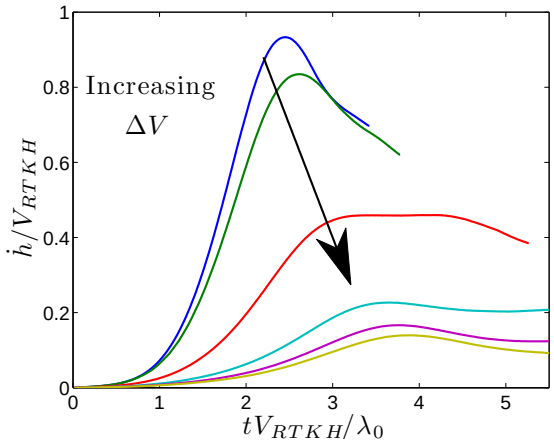

FIG. 5: Mixing rate for the combined RT/KH instability. The same cases as in Fig. 4 but scaled by the combined velocity scale V_{RTKH}.

from (1) by the wavenumber magnitude k yields

$$\frac{\gamma}{k} = \sqrt{\frac{1-A^2}{4}\left(\frac{k_x}{k}\right)^2 V_{KH}^2 + \frac{k_0}{2\pi k} V_{RT}^2}\,,$$

where the velocity scales for pure RT and KH have been used. For broadband perturbations in 3D this must be integrated over all orientations k_x/k and magnitudes k. However, since streamwise modes grow fastest, it is reasonable to assume that k_x/k approaches 1 after some time. Similarly, the growth rate is primarily given by modes around the peak, i.e., with $k \approx k_0$. We then get (with a factor of $\sqrt{2\pi}$ taken out for convenience)

$$\sqrt{2\pi}\,\frac{\gamma}{k} \approx \sqrt{\frac{(1-A^2)\pi}{2} V_{KH}^2 + V_{RT}^2} \equiv V_{RTKH}\,,$$

which we take as the velocity scale for the combined RT/KH problem.

Figure 5 shows the growth rate $\dot{h}$ for the same cases, but now with both $\dot{h}$ and time scaled by the combined velocity scale. With this scaling the growth rates fall in an enveloped region with pure RT at the top and pure KH at the bottom. Note that there is a certain degree of collapse in the temporal direction, and that the shape of the curves are somewhat similar. The similarity of the shapes leads us to characterize each curve by a single number, which we take as the peak growth rate $\dot{h}_{\max}$. Figure 6 shows this quantity (scaled by V_{RTKH}) versus the parameter $\beta \equiv V_{RT}/V_{RTKH}$. Note that β is 1 for pure RT and 0 for pure KH mixing, and hence it is a measure of the relative importance of each phenomenon. The collapse of the peak growth rates onto a single curve is surprisingly good.

To investigate why the data collapse as well as they do, we note that dimensional analysis suggests that $\dot{h}_{\max}$ is a function of V_{RT}, V_{KH} and A (the other parameters from which a velocity scale can be formed, g and λ_0, are included in V_{RT}). This can be written as,

$$\dot{h}_{\max} = V_{RTKH} \cdot f\left(\frac{V_{RT}}{V_{RTKH}}, A\right)\,,$$

where f is some unknown function. Note that the first argument of f is exactly β; in fact, that was why β was chosen that way in the first place. The collapse of the scaled maximum growth rates in Fig. 6 suggests that the dependence on A in f is minor, and hence the maximum growth rate can be approximated well as $\dot{h}_{\max} \approx V_{RTKH} \cdot \tilde{f}(\beta)$, where $\tilde{f}$ is a reasonably universal function.

We can now attempt to answer one of the questions raised earlier: given fixed RT-parameters, what amount of shear minimizes the growth rate? This question amounts to minimizing

$$\frac{\dot{h}_{\max}}{V_{RT}} = \frac{\tilde{f}(\beta)}{\beta}\,,$$

which is shown in Fig. 7. The minimum occurs at $\beta_{\text{opt}} \approx 0.4$.

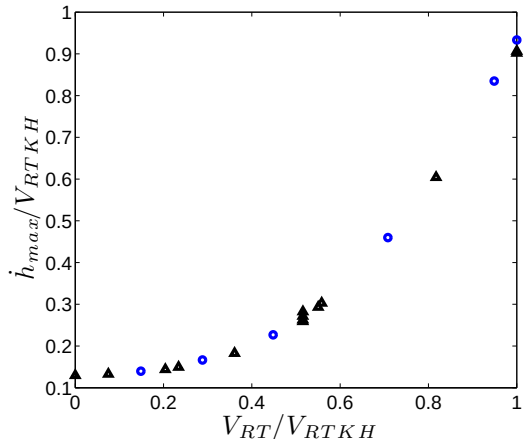

FIG. 6: Peak growth rate in the combined RT/KH instability as a function of $\beta = V_{RT}/V_{RTKH}$. Blue circles denote the 6 cases in Figs. 4 and 5 with fixed RT-parameters ($A = 0.5$)and increasing shear, whereas the black triangles denote the remaining 14 cases with different RT and KH parameters. Five of these cases had Atwood numbers of $1/3, 1/3, 3/5, 2/3, 5/7$ for β values of $.52, 1.0, .52, .52, 1.0$, respectively.

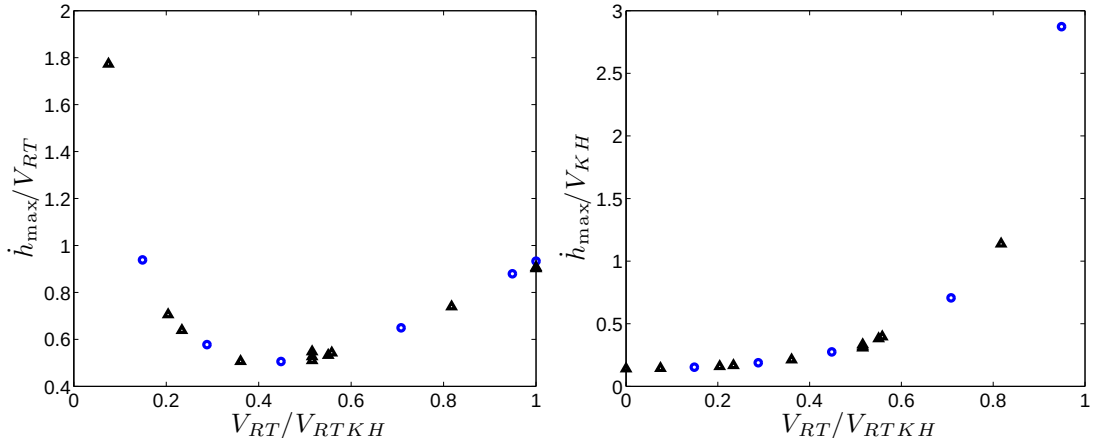

FIG. 7: Maximum mixing rate $\dot{h}_{\max}$ for fixed RT (left) and fixed KH (right) parameters as functions of the relative amount of each instability $\beta = V_{RT}/V_{RTKH}$. Symbols as in Fig. 6.

The opposite question is whether for fixed KH-parameters it is possible to find non-zero RT parameters that minimize the growth rate? This question amounts to minimizing

$$\frac{\dot{h}_{\max}}{V_{KH}} = \sqrt{\frac{(1-A^2)\pi}{2}}\,\frac{\tilde{f}(\beta)}{\sqrt{1-\beta^2}}\,,$$

which is also shown in Fig. 7. It is clear that, unlike with adding shear, the addition of gravity monotonically increases the mixing rate, exactly as predicted by linear stability theory.

IV. MIXING RATE AND THE VERTICAL MASS FLUX

Given the non-monotonic behavior of $\dot{h}$ with increasing shear-addition, it is instructive to examine this metric more closely in order to trace the origins of the non-monotonicity. We first note that the mean density profile $\overline{\rho}(z,t)$ is observed to be monotonic in z at all times, and hence we can write the mixing-height h, defined in (4), as

$$h(t) = \frac{2}{\Delta\rho}\int_{-\infty}^{z_0(t)} (\overline{\rho} - \rho_L)\, dz + \frac{2}{\Delta\rho}\int_{z_0(t)}^{\infty} (\rho_H - \overline{\rho})\, dz\,,$$

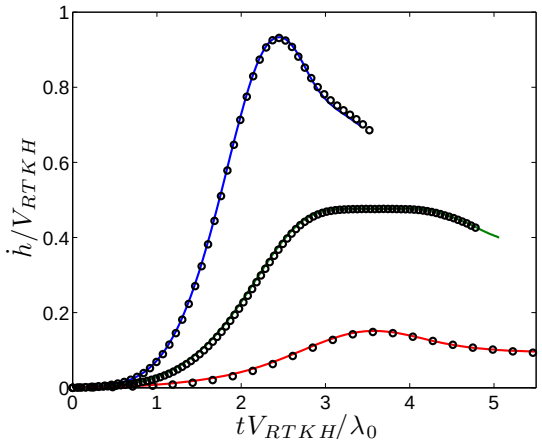

FIG. 8: Comparison of $\dot{h}(t)$ (lines) and $-4\overline{\rho' w'}(z_0,t)/\Delta\rho$ (circles) from (7) for three cases with $\beta = 1.0$, 0.71, and 0.15 and $A = 0.5$.

where $z_0(t)$ is the vertical half-point between the two densities, i.e., $\overline{\rho}(z_0(t),t) = (\rho_L + \rho_H)/2$. Taking the time-derivative of h then yields

$$\dot{h}(t) = \frac{2}{\Delta\rho}\int_{-\infty}^{z_0(t)} \frac{\partial\overline{\rho}}{\partial t} dz - \frac{2}{\Delta\rho}\int_{z_0(t)}^{\infty} \frac{\partial\overline{\rho}}{\partial t} dz\,,$$

where the remaining terms in Leibniz's integral rule (terms including $\partial z_0/\partial t$) cancel out. The equation for conservation of mass (2a) can then be used to replace $\partial\overline{\rho}/\partial t$ by $-\partial\overline{\rho w}/\partial z$. Integrating in z then yields, with $\overline{\rho w} = 0$ at $z = \pm\infty$,

$$\dot{h}(t) = -4\frac{\overline{\rho w}(z_0,t)}{\Delta\rho} \approx -4\frac{\overline{\rho' w'}(z_0,t)}{\Delta\rho}\,, \tag{7}$$

where the approximation $\overline{\rho w} \approx \overline{\rho' w'}$ is used; note that DNS and LES results show that this is a very good approximation. The primes indicate fluctuating quantities, where variables have been decomposed as $\Phi(x,y,z,t) = \overline{\Phi}(z,t) + \Phi'(x,y,z,t)$. To verify the accuracy of this relation, we plot for three cases the left and right hand sides of (7) in Fig. 8. There is no appreciable difference between the two curves, and we can therefore conclude that mixing rate is proportional to the planar-averaged vertical turbulent mass flux taken at $z = z_0(t)$. The turbulent vertical mass flux can also be written in terms of a correlation coefficient and the individual rms-values as

$$\overline{\rho' w'} = R_{\rho' w'}\rho'_{\rm rms} w'_{\rm rms}\,. \tag{8}$$

Fig. 9 shows the three factors in this relation at height z_0 at the time of peak mixing rate. As $\beta = V_{RT}/V_{RTKH}$ decreases, both $\rho'_{\rm rms}$ and the correlation coefficient $R_{\rho' w'}$ decrease monotonically. In contrast, the vertical velocity fluctuation $w'_{\rm rms}$ shows a non-monotonic behavior with a minimum around $\beta \approx 0.6$. This shows that the non-monotonic behavior of the mixing rate has its roots in the vertical component of the turbulence kinetic energy, and how this changes with the addition of mean shear. We therefore look more closely at the budget of this quantity.

V. ENERGY BUDGET AND MIXING EFFICIENCY

To gain more insight into the non-monotonic behavior of the vertical kinetic energy $\overline{w'w'}$, we want to look at the energy budget for this quantity. As outlined in the previous section, the link to the mixing rate is through the kinetic energy at the mixing half-point, i.e., $\overline{w'w'}(z_0,t)$. However, the budget for a global vertical kinetic energy K'_V (to be defined below) is more easily both defined and interpreted. We therefore proceed by first proposing and verifying a relationship between $\overline{w'w'}(z_0,t)$ and K'_V, which then allows us to consider a global energy budget for K'_V.

When averaged in the horizontal directions and integrated in the vertical z direction (over L), the energy equation becomes

$$\frac{d}{dt}\int_L \frac{\overline{\rho u_i u_i}}{2} dz = -\frac{d}{dt}\int_L \overline{\rho} g z dz - \int_L \overline{\tau_{ij}\frac{\partial u_i}{\partial x_j}} dz \tag{9}$$

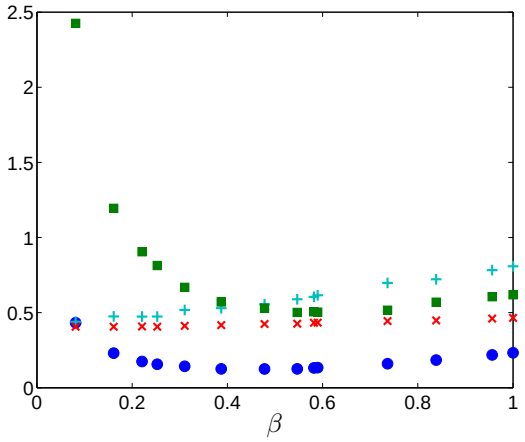

FIG. 9: Factors in Eqn. 8 as functions of $\beta = V_{RT}/V_{RTKH}$ evaluated at z_0 at the time of peak mixing rate: $-\overline{\rho' w'}/\Delta\rho V_{RT}$ (blue circles), $-R_{\rho' w'}$ (cyan plusses), $\rho'_{\rm rms}/\Delta\rho$ (red crosses), and $w'_{\rm rms}/V_{RT}$ (green squares).

where the negligible pressure dilation term, $\int_L \overline{p\frac{\partial u_i}{\partial x_i}} dz$,has been omitted as in [8]. Define the vertical turbulent kinetic energy, the horizontal mean and turbulent kinetic energy, and the gravitational potential energy as

$$\begin{aligned} K'_V &= \frac{1}{2}\int_L \overline{\rho\, w' w'}\, dz\,, \\ \overline{K}_H &= \frac{1}{2}\int_L \overline{\rho}\,\overline{u}^2\, dz\,, \\ K'_H &= \frac{1}{2}\int_L \overline{\rho u' u'}\, dz \\ P &= \int_L \overline{\rho}\, g z\, dz\,, \end{aligned}$$

and then define $K_{\rm rem}$ as the sum of all remaining terms in the kinetic energy. $K_{\rm rem}$ was below 3.5% of the total kinetic energy for all cases and time and will henceforth be neglected. We next define the energy released from the mean velocity and density fields as [8]

$$\begin{aligned} \delta\overline{K}_H &= \overline{K}_H(0) - \overline{K}_H(t)\,, \\ \delta P &= P(0) - P(t)\,, \end{aligned}$$

and the energy dissipated into heat as

$$\Psi = \int_0^t \int_L \overline{\tau_{ij}\frac{\partial u_i}{\partial x_j}}\, dz dt'\,.$$

Integrating (9) in time then yields the global energy budget

$$K'_V + K'_H + \Psi \approx \delta P + \delta\overline{K}_H\,, \tag{10}$$

where energy released from the mean fields (right-hand-side) is partitioned between vertical turbulent kinetic energy, horizontal turbulent kinetic energy and heat. The approximation sign is used as the analysis neglects the small ($< 4\%$) terms.

We must next establish a link between K'_V and $\overline{w'w'}(z_0,t)$. Since the latter quantity was shown in Section IV to be responsible for the non-monotonic behavior of the mixing rate, this would tie K'_V to the non-monotonic behavior. The shape in z of $\overline{w'w'}$ is nearly constant in time (approximately resembling a Gaussian), with a width that scales with the mixing-height $h(t)$ and a peak value that scales with $\overline{w'w'}(z_0,t)$. Hence

$$\frac{K'_V(t)}{h(t)} \approx C\frac{\rho_1+\rho_2}{2}\,\overline{w'w'}(z_0,t) \tag{11}$$

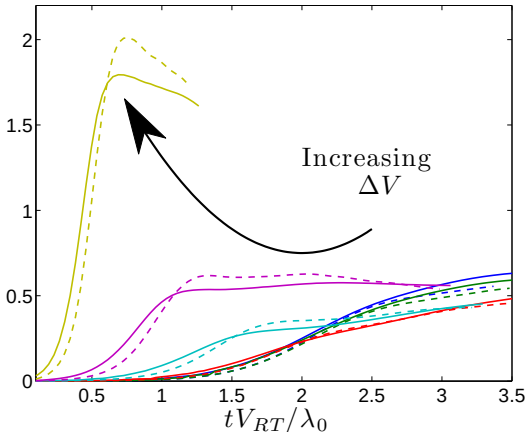

FIG. 10: Verification of the approximate relation (11) between global and local vertical kinetic energy. Comparison of $K_V'/h(t)$ (solid) and $0.5C(\rho_1+\rho_2)\overline{w'w'}(z_0,t)$ (dashed) for 6 cases with fixed RT-parameters and increasing shear. The curves are scaled by $V_{RT}^2(\rho_1+\rho_2)/2$.

is an approximative relation between the global $K_V'(t)$ and the local $\overline{w'w'}(z_0,t)$. Figure 10 shows both sides of this relation for $C = 1.1$. There is clearly a strong correlation between the curves. The error in the approximative relationship (11) can be quantified as the difference between the left- and right-hand sides, normalized by the average of the two. At the time of peak mixing rate, this error is below 0.085 for all 20 cases. It is clear that the global measure K_V' well captures the non-monotonic behavior.

Up to this point it has been shown that the mixing rate $\dot{h}(t)$ is very well approximated by the turbulent mass-flux at the interface $\overline{\rho'w'}(z_0,t)$, that the non-monotonicity in this mass-flux is due to $\overline{w'w'}(z_0,t)$ at the interface, and finally that this local vertical kinetic energy can be reasonably approximated by the global vertical kinetic energy $K_V'(t)$. The energy budget (10) is useful to illuminate the cause of the non-monotonicity. Consider keeping the RT-parameters fixed while increasing the mean shear (thus lowering β); this would monotonically increase the amount of energy available for release from the mean flow. The non-monotonicity of K_V' then implies that the efficiency at which energy is channeled into vertical fluctuations decreases with increasing amounts of mean shear. This can be quantified by defining a vertical mixing efficiency

$$\eta_V \equiv \frac{K_V'}{\delta P + \delta\overline{K}_H},$$

which measures how much of the total amount of energy released into the flow contributes to vertical mixing of the interface. Figure 11 shows this quantity for a range of cases with increasing shear. The efficiency decreases quite dramatically, by about a factor of two, when going from pure RT to pure KH mixing. It is this decrease that causes the mixing rate to decrease when small amounts of shear are added. This behavior should perhaps not be surprising, since gravitational acceleration is directed in the vertical direction whereas shear acts in the horizontal direction.

VI. FLOW STRUCTURES

Figure 12 shows a visualization of the vortical structures in the mixing region at the time of peak mixing rate for a set of cases. Note that the density has been used to color the structures; hence red areas should be interpreted as areas of downward motion of heavy fluid. It is clear that the structure of the motions changes dramatically from the pure RT to the pure KH problems. Pure Rayleigh-Taylor mixing has essentially circular vortices surrounding the characteristic bubbles and spikes. As shear is added, the structures become progressively more two-dimensional, with large rollers in the spanwise direction that are connected through small braids. This change in flow structure appears gradual and monotonic.

This reshaping of the structures can also be seen in the spectra of density at the half-point $z = z_0$, as shown in Fig. 13. For pure RT mixing ($\beta = 1$), the spectra in the x and y directions are identical, with a peak around wavenumber k_0. As the amount of shear is increased, there appears a secondary peak around $k_x \approx 2k_0$ in the streamwise spectrum, and simultaneously the peak in the spanwise spectrum moves towards lower wavenumbers. We recall that the mixing rate $\dot{h}$ has its minimum for $\beta \approx 0.4$, at which point the flow closely resembles the pure KH case (secondary peak has appeared, spanwise peak started moving towards lower wavenumbers). Thus it makes intuitive

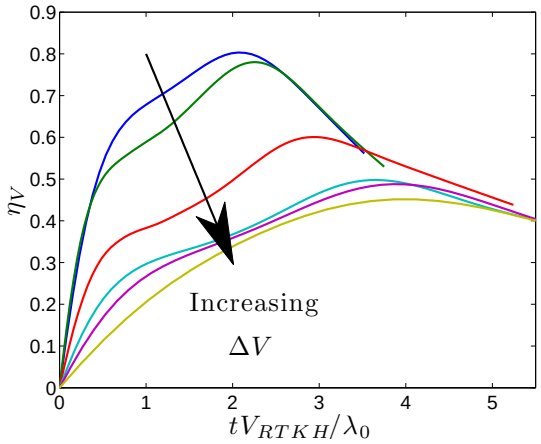

FIG. 11: Vertical mixing efficiency η_V versus time for 6 cases with fixed RT parameters and increasing shear.

sense that any further addition of shear past this point would begin increasing the mixing rate, as more energy is released into the flow.

Finally, Fig. 14 shows density contours in planes for increasing amounts of shear. Qualitatively, the case with the minimum peak mixing rate has clearly changed from the pure RT structure towards the characteristic KH structure.

VII. SUMMARY

The combined Rayleigh-Taylor/Kelvin-Helmholtz instability is studied mainly through LES. While linear stability theory predicts that the growth rate should increase monotonically with both increasing amounts of shear (for fixed gravitational parameters) and increasing amounts of gravity (for fixed shear parameters), the simulations in the early nonlinear regime show a more complex and non-monotonic behavior. With fixed RT parameters, addition of a small amount of mean shear actually decreases the nonlinear mixing rate during the early nonlinear stage. The peak mixing rate reaches a minimum around $\beta \equiv V_{RT}/V_{RTKH} \approx 0.4$. Thus the optimum amount of shear (that minimizes the peak mixing rate for fixed RT parameters) is $\Delta V_{\rm opt} \approx 1.8\sqrt{Ag\lambda_0/(1-A^2)}$.

The analysis, both quantitative and visual, suggests that the addition of a small amount of shear changes the structure of the instability such that less energy is channeled into vertical mixing. At the point of minimum peak mixing rate, the structure has changed to largely resemble a pure KH instability. Further increasing the shear then simply increases the amount of energy available, and thus increases the mixing rate again.

Acknowledgments

This work has been supported by the DOE Scientific Discovery through Advanced Computing (SciDAC) program and the DOE Computational Science Graduate Fellowship (CSGF) with computational support from the DOE NERSC and ALCF facilities (through the ERCAP and INCITE programs, respectively) and through the LLNL HPC Center. This work was also performed under the auspices of the U.S. Department of Energy by Lawrence Livermore National Laboratory under Contract No. DE-AC52-07NA27344.

[1] P.G. Drazin, *The stability of a shear layer in an unbounded heterogeneous inviscid fluid*, J. Fluid Mech., **4**, 214 (1958).
[2] S. Chandrasekhar, Hydrodynamic and Hydromagnetic Stability, Int. Ser. Monographs on Physics, Clarendon Press, Oxford (1961).
[3] P. N. Guzdar, P. Satyanarayana, J. D. Huba and S. L. Ossakow *Influence of Velocity Shear on the Rayleigh-Taylor Instability*, Geophysical Research Letters, **9**, No. 5, pp 547-550 (1982).
[4] T. Gerz, U. Schumann and S.E. Elghobashi, *Direct numerical simulation of stratified homogeneous turbulent shear flows*, J. Fluid Mech., **200**, pp. 563-594

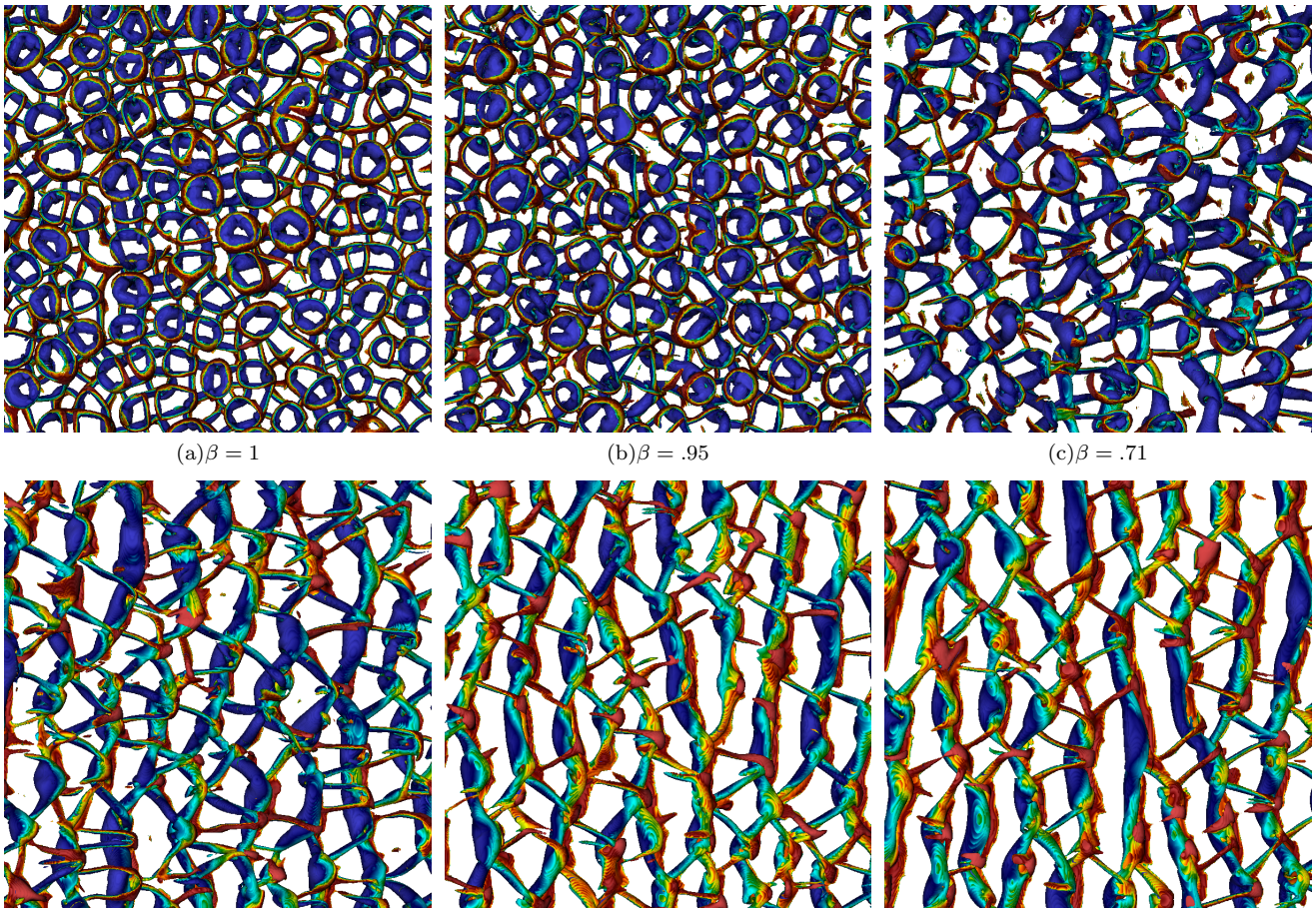

(a)$\beta = 1$ (b)$\beta = .95$ (c)$\beta = .71$

(d)$\beta = .45$ (e)$\beta = .28$ (f)$\beta = .15$

FIG. 12: Vortical structures in the mixing region at the time of peak mixing rate for cases with identical RT parameters but varying amounts of shear (different β). Iso-surfaces of the intermediate eigenvalue $\lambda_2 = 0$, colored by density from heavy (red) to light (blue) fluid. Only one-quarter of the domain is shown.

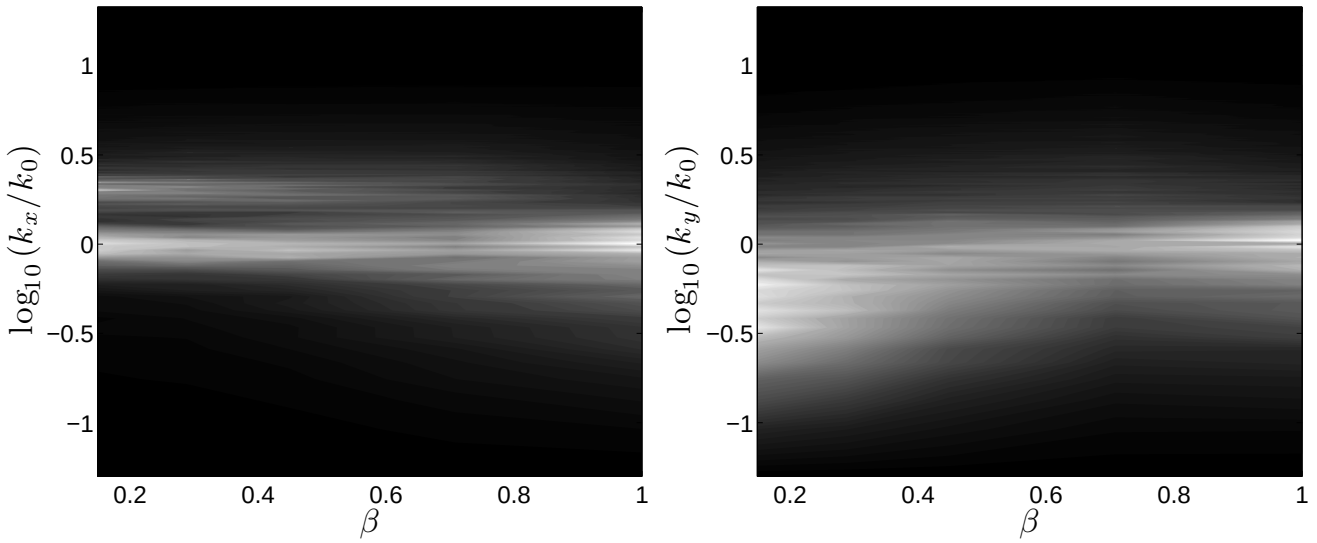

FIG. 13: Contours of the pre-multiplied density spectra in the x (left) and y (right) direction at the half-point $z = z_0$ at the time of peak mixing rate, with light regions showing higher spectral energy density. The horizontal axes denote relative amount of shear (through β), while the vertical axes denote the wavenumber in the direction of mean shear (left image) and normal to it (right).

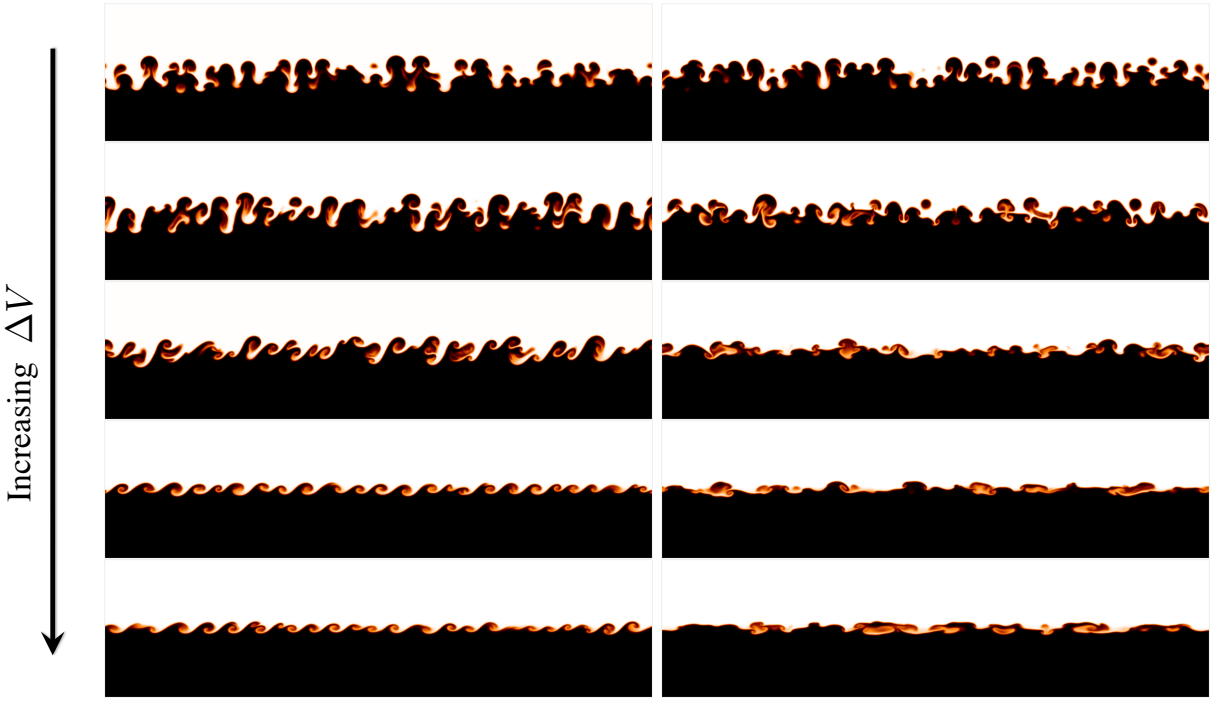

FIG. 14: Density contours of cases with increasing amounts of shear, $\beta = [1, .71, .45, .28, .15]$, (top to bottom) at the time of peak mixing rate in the x (left) and y direction (right). Note that the middle row is $\beta \approx 0.45$, near the optimum amount of shear.

[5] G. Velarde, Y. Ronen and J. M. Martnez-Val, Nuclear fusion by inertial confinement: a comprehensive treatise, CRC Press Inc., pp. 20-25, (1993).

[6] D. D. Joseph, *Fluid Dynamics of Two Miscible Liquids with Diffusion and Gradient Stresses*, Eur. J. Mech. B/Fluids 9, 565-596 (1990)

[7] A. W. Cook and P. Dimotakis, *Transition stages of RayleighTaylor instability between miscible fluids*, J. Fluid Mech., **443**, pp. 6999 (2001).

[8] W. H. Cabot and A. W. Cook, *Reynolds number effects on Rayleigh-Taylor instability with possible implications for type-1a supernovae*, Nature Physics, Volume 2, August 2006

[9] A. W. Cook, *Artificial Fluid Properties for large-eddy simulation of compressible turbulent mixing*, Phys. Fluids, **19**, 055103 (2007).

[10] N. J. Mueschke and O. Schilling, *Investigation of RayleighTaylor turbulence and mixing using direct numerical simulation with experimentally measured initial conditions. I. Comparison to experimental data*, Phys. Fluids, **21**, 014106 (2009).

[11] U. Shumlak and N. F. Roderick, *Mitigation of the Rayleigh-Taylor instability by sheared axial flows*, Phys. Plasmas, **5**, 6 (1998).

[12] W. Zhang, Z. Wu and D. Li, *Effect of shear flow and magnetic field on the Rayleigh-Taylor instability*, Phys. Plasmas, **12**, (2005).

[13] D. M. Snider and M. J. Andrews, *Rayleigh-Taylor and shear driven mixing with an unstable thermal stratification*, Phys. Fluids, **6**, 10 (1994).

[14] S.K. Lele, *Compact Finite-Difference Schemes With Spectral-Like Resolution*, J. of Comp. Phys., **103**, 16 (1992).